Volume 18, Number 4, 2025. pp. 455-466

Jordan Journal of Physics

ARTICLE

# Analysis of Generating a Microwave Frequency Comb in Laser-Assisted Scanning Tunneling Microscopy with a Semiconductor Sample

**Marwan S. Mousa**[a] and **Mark J. Hagmann**[b]

[a] *Department of Renewable Energy Engineering, Jadara University, Irbid 21110, Jordan.*
[b] *Department of Electrical and Computer Engineering, University of Utah, Salt Lake City, Utah, 84112, USA.*

***Doi:*** **https://doi.org/10.47011/18.4.4**
*Received on: 30/05/2024;* *Accepted on: 20/10/2024*

**Abstract:** When a mode-locked laser is focused on the tunneling junction of a scanning tunneling microscope optical rectification generates microwave harmonics at integer multiples of the laser pulse repetition frequency. These harmonics set the present state-of-the-art for a narrow-linewidth microwave source because of the high stability of passive mode-locking in the laser. Hundreds of harmonics are measured with a signal-to-noise ratio exceeding 25 dB with a metal sample in the STM. However, the harmonics are attenuated by the spreading resistance with a resistive sample. Now the spreading resistance is quantified and analysis with equivalent circuit models is used to characterize the effects to support further measurements with semiconductors.

**Keywords:** Microwave frequency comb, Microwave source, Mode-locked lazer.

## 1. Introduction

We have previously generated a microwave frequency comb (MFC) by focusing a mode-locked laser on the tunneling junction of a scanning tunneling microscope (STM) with a metallic sample electrode. For example, the 200$^{th}$ harmonic at a frequency of 14.85 GHz, which is 200 times the laser pulse repetition frequency, has a power of -145 dBm, which is 25 dB above the displayed average noise level (DANL) [1]. Each harmonic has a linewidth less than 0.1 Hz, setting the present state of the art for a narrow linewidth microwave source [2]. Thus, the quality factor (Q) of the 200$^{th}$ harmonic exceeds 1.5x10$^{11}$. For comparison, the Q is typically 100 for resonant circuits with discrete components, 10$^6$ for metal microwave cavities, and 10$^9$ for superconductive microwave cavities. We attribute the extremely narrow linewidth to the high stability of the mode-locked laser, noting that if the laser pulse train were exactly periodic, the linewidth would be zero, so the Q would be infinite. With metal samples, the power at each harmonic is inversely proportional to the square of its frequency. We attribute this roll-off to shunting by the capacitance (≈ 6 pF) between the leads for the tip and sample, but within the tunneling junction, the harmonics may extend to terahertz frequencies [3].

In our first measurements of the MFC with a semiconductor, we used intrinsic (n-type) gallium nitride (GaN). As the DC bias for the STM was slowly increased, the harmonics were first seen at a value of 9 V at which the DC tunneling current was 1 μA. Then, as the bias was reduced, the harmonics continued until reaching 5 V. We measured the first five harmonics of the MFC in 1,062 scans of the spectrum analyzer over a duration of 43 minutes. However, after that, it was not possible to see the harmonics [4]. We have seen the harmonics in more recent measurements, but they do not have

**Corresponding Author:** Marwan S. Mousa **Email**: m.mousa@jadara.edu.jo

the stability that is found with metallic samples. The analysis in this paper was made with the objective of understanding and optimizing our measurements with semiconductors.

## 2. Modeling Spreading Resistance in the Semiconductor

The electrical resistance between a small contact at the surface of an object with resistivity ρ and a second contact with much greater area is called the "spreading resistance" and is independent of the location and size of the larger contact. The spreading resistance is given by ρ/4a, where "ρ" is the resistivity of the object, "a" is the radius of the contact, and the object is much larger than a [5]. We previously extended the Simmons analysis of quantum tunneling between two infinite parallel flat metal plates [6] to approximate the distribution of the tunneling current on a metallic sample in an STM by modeling the tip as a metal sphere with a flat metal plate as the sample [7]. Now, in Appendix I, we extended this method to approximate the spreading resistance in the resistive sample of an STM. Examples of these calculations are shown in Figs. 1 and 2.

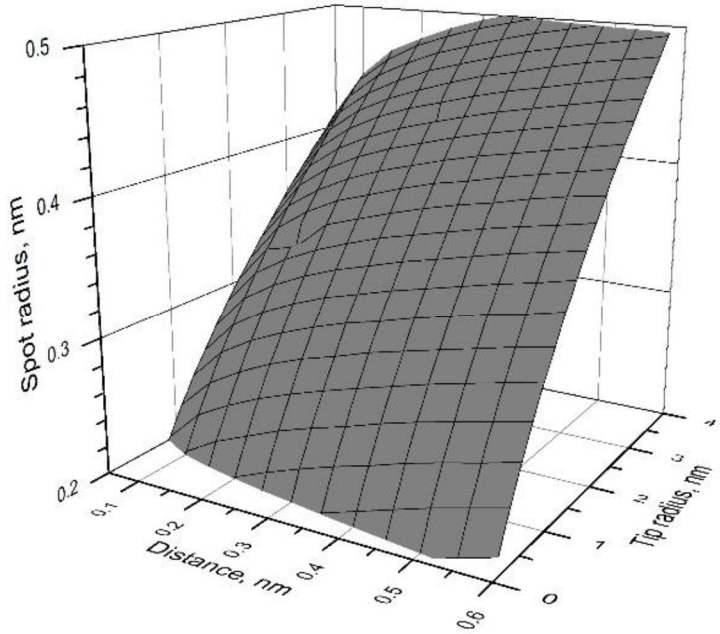


FIG. 1. Spot radius for the tunneling current.

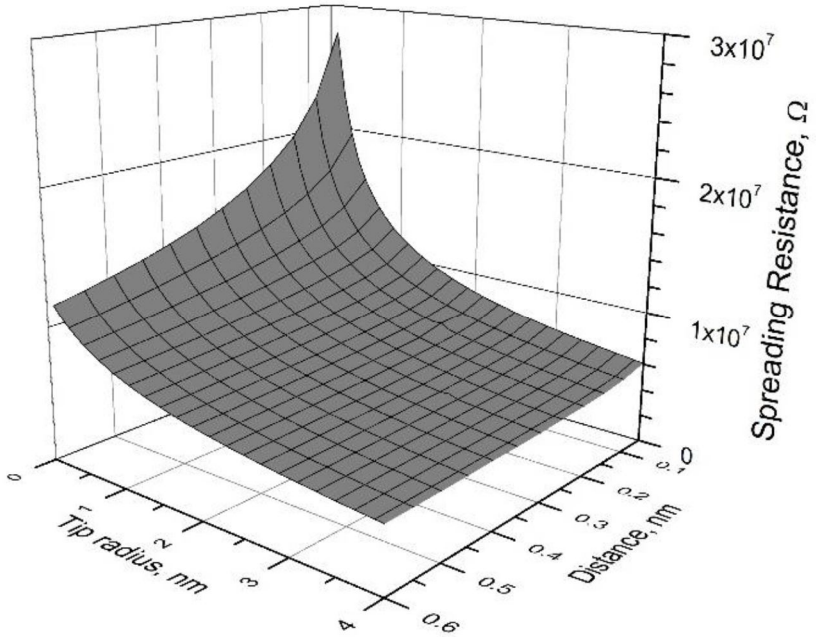


FIG. 2. Spreading resistance for the tunneling current.

Figure 1 shows the effective spot radius "a" calculated for the tunneling current at the surface of a resistive sample in an STM as a function of the tip-sample distance and the tip radius. Figure 2 shows the spreading resistance, which is proportional to the resistivity, for a sample resistivity of 1 Ω-cm. Figure 2 shows that the spreading resistance is increased by reducing the radius of the tip or the tip-sample distance. The axial extent of the contribution to the spreading resistance within the sample is comparable to the spot radius. The resolution is measured by laser-assisted scanning tunneling microscopy may be much finer than the spot size because the laser radiation is focused to a finer size by the tip, which acts as an optical antenna. By analogy, sub-nanometer resolution is already achieved in tip-enhanced Raman spectroscopy because of near-field intensification of the laser radiation by the tip [8].

## 3. Delimitations in the Measurement and Analysis of the MFC with a Semiconductor Sample

Figure 3 is a block diagram of the apparatus we have used to measure the MFC with a semiconductor as the sample in a commercial STM (UHV 300, from RHK Technology) at Los Alamos National Laboratory. With a metallic sample, the MFC is measured by connecting a spectrum analyzer to a Bias T inserted between the sample and the bias supply. However, with a semiconductor, each laser pulse generates a pulse of carriers that has a comparable duration (e.g., 15 fs), and simulations show that the carrier pulse undergoes severe attenuation and dispersion as it moves outward from the tip through the semiconductor [9]. Thus, the harmonics are only seen with a surface probe that is close to the tunneling junction as shown in Fig. 3. It would be simpler to measure the harmonics between the tip and the preamplifier for the STM control electronics but a Bias-T or miniature transformer inserted at that point interferes with feedback control of the tunneling current in the commercial STM to cause the tunneling current to be unstable. A rigorous analysis of the MFC with a semiconductor sample would require modeling the transport of carriers from the tunneling junction to the surface probe [9]. However, to simplify the calculations, we assume that this probe is close enough to the tip that no correction is required for attenuation and dispersion of the carriers after they have passed through the spreading resistance. In the analysis, we assume that the photon energy for the laser is less than the bandgap energy of the semiconductor to prevent surge currents caused by the formation of electron-hole pairs, which interfere with measuring the MFC [10]. We also neglect other photon processes that may occur within the semiconductor.

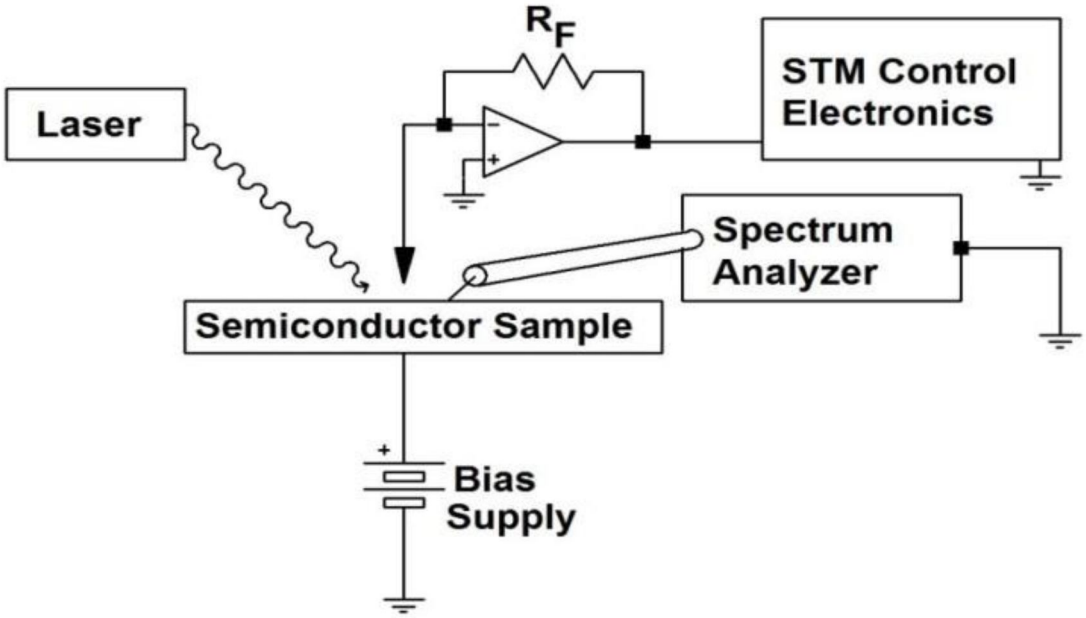


FIG. 3. Block diagram for measuring the MFC with a semiconductor in the STM.

## 4. Procedure for Simulations Based on the Derivations in the Appendices

*4.1 Method to Determine the Operating Point with Example*

First, it is necessary to determine the DC tunneling current IDC and the tip-sample distance d when the DC bias voltage VB, the effective emitting area of the tip A, and the work function φ are specified, by using procedures that are described in Appendix I. The DC equivalent circuit model for the tunneling junction of an STM with a resistive sample consists of the applied DC bias VB in series with the tunneling resistance RT and the spreading resistance of the sample RS. The tunneling resistance is defined by RT ≡ VTS/IDC, where VTS is the tip-sample voltage and IDC is the DC tunneling current. We use Eq. (1) to approximate the DC tunneling current, where the parameters α and β are given in Eqs. (2) and (3) [6]. Thus, the tunneling resistance is given by Eq. (4).

$$I_{DC} = \frac{\alpha A V_{TS}}{d} e^{-\beta d} \quad (1)$$

$$\alpha = \sqrt{2m\phi_M e}\left(\frac{e}{h}\right)^2 \quad (2)$$

$$\beta = \frac{4\pi}{h}\sqrt{2m\phi_M e} \quad (3)$$

$$R_T = \frac{d}{\alpha A} e^{\beta d} \quad (4)$$

Equation (5) from Appendix I is used to determine the spreading resistance RS, where functions F1(R) and F2(R,ρ) are defined in Eqs. (6) and (7).

$$R_S = F_2(R,\rho) \cdot e^{F_1(R).d} \quad (5)$$

$$F_1(R) = 4.773 \times 10^9 + 2.480 \times 10^8 Ln(R) \quad (6)$$

$$F_2(R,\rho) = \frac{2462\rho}{R^{0.400}} \quad (7)$$

Thus, the DC tunneling current is given by Eq. (8), which may also be written in the form of Eq. (9). We solve Eq. (9) iteratively by the method of bisection to determine the tip-sample distance d and then use Eq. (1) to determine IDC. Gaussian noise is added to simulate the measured current, which is reported to the user. However, the values of A, φ, and d are unknown to the user.

$$I_{DC} = \frac{V_B}{R_S + R_T} = \frac{V_B}{F_2(R,\rho)\cdot e^{F_1(R).d} + \frac{d}{\alpha A} e^{\beta d}} \quad (8)$$

$$F_2(R,\rho) \cdot e^{F_1(R).d} + \frac{d}{\alpha A} e^{\beta d} - \frac{V_B}{I_{DC}} = 0 \quad (9)$$

Figure 4, which was prepared by following this procedure, shows the simulated tip-sample distance d as a function of the current IDC for sample resistivities of 0, 0.001, 0.01, 0.1, 1, and 10 Ω-cm with a tungsten tip having an apex radius of 0.3 nm and a DC bias of 1 V. Note that for each value of the resistivity the curve deviates from that for zero resistivity as the current is increased because the voltage drop across the spreading resistance is greater.

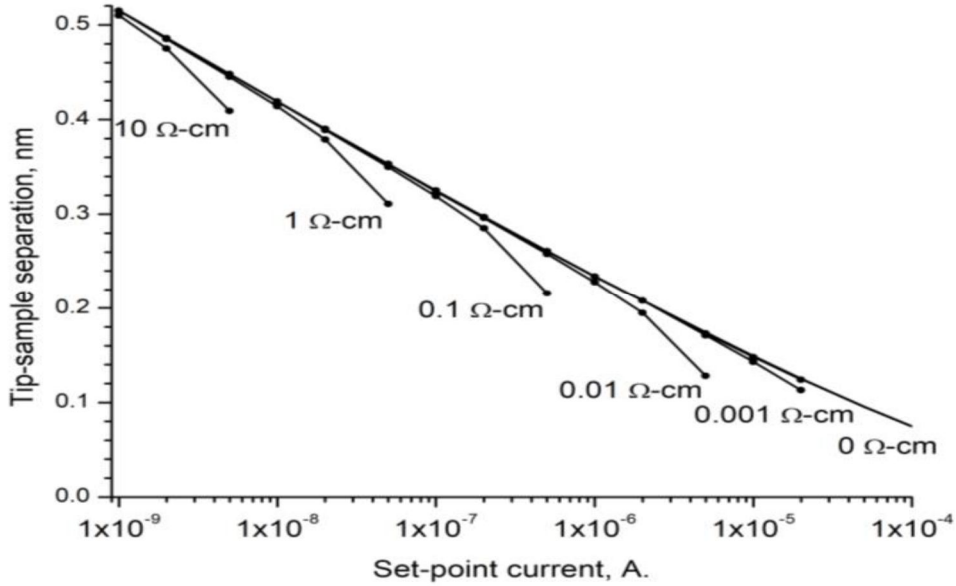


FIG. 4. Tip-sample distance vs. current for an applied bias of 1 V, and sample resistivities of 0, 0.001, 0.01, 0.1, 1, and 10 Ω-cm, from the top curve to the lower one.

### *4.2 Simulations of the Power at the Microwave Harmonics*

In Appendix II, it is shown that the microwave power at each harmonic is given by Eq. (10), where the prefactor K depends on the nonlinear relationship of the tunneling current to the applied voltage, the power and focusing of the laser, and the harmonic number. In our simulations, we use K =1.44x10$^{-34}$ W-mtr$^2$, which is based on our many measurements for the case ρ = 0 with metal samples [1].

$$P = \frac{Ke^{-2\beta d}}{d^2\left(1+\frac{R_S}{R_T}\right)^4} \tag{10}$$

## 5. Results of the Simulations

Figure 5 shows the simulated microwave power as a function of the applied DC bias and the DC tunneling current that were calculated using ρ = 0.1 Ω-cm in Eq. (10). Note that the microwave power is maximum and remains constant for a specific set of values for VDC and IDC.

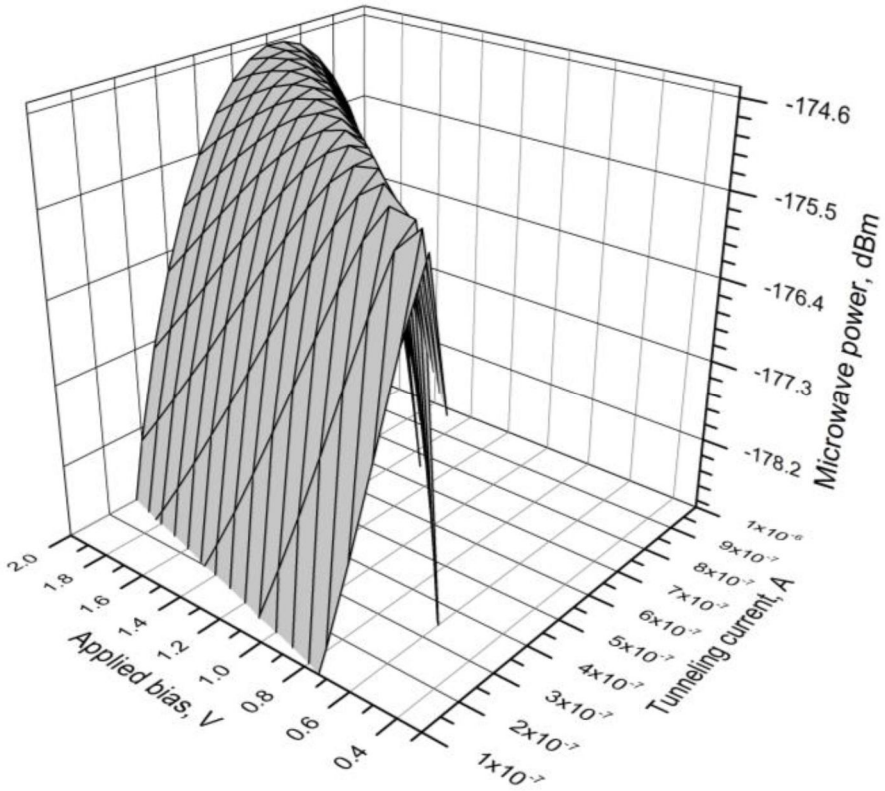


FIG. 5. Microwave power vs. applied DC bias and DC tunneling current as calculated using Eq. (10) with ρ = 0.1 Ω-cm.

Figure 6 shows the simulated microwave power as a function of the DC tunneling current ISP for ρ = 0.1 Ω-cm in Eq. (10) with DC bias values of 0.5, 1.0, 1.5, 2.0, and 2.5 V. Note that this is a cut through the "ridge" that is seen in Fig. 5 for specific values of the DC bias voltage. This figure shows that the microwave power is maximum and remains constant for a specific set of values for the bias voltage. Again, in Figs. 5 and 6, the calculations were made for a tungsten tip having an apex radius of 0.3 nm and a DC bias of 1 V. A "ridge" similar to that in Fig. 5, where the microwave power is maximum and constant, is also seen with other values of the sample resistivity. Fig. 7 shows the microwave power for each value of the sample resistivity when the applied DC bias and the DC tunneling current are chosen to obtain the maximum power for that resistivity. We have recently developed a low-noise solid-state preamplifier that increases the signal-to-noise ratio in these measurements by 14 dB with our spectrum analyzer. Thus, the displayed average noise level (DANL) may be reduced from -170 dBm (seen in Fig. 3) to as low as -184 dBm, as shown in Fig. 7. As noted earlier, the extremely narrow linewidth of the microwave harmonics makes it possible to measure attowatt level signals.

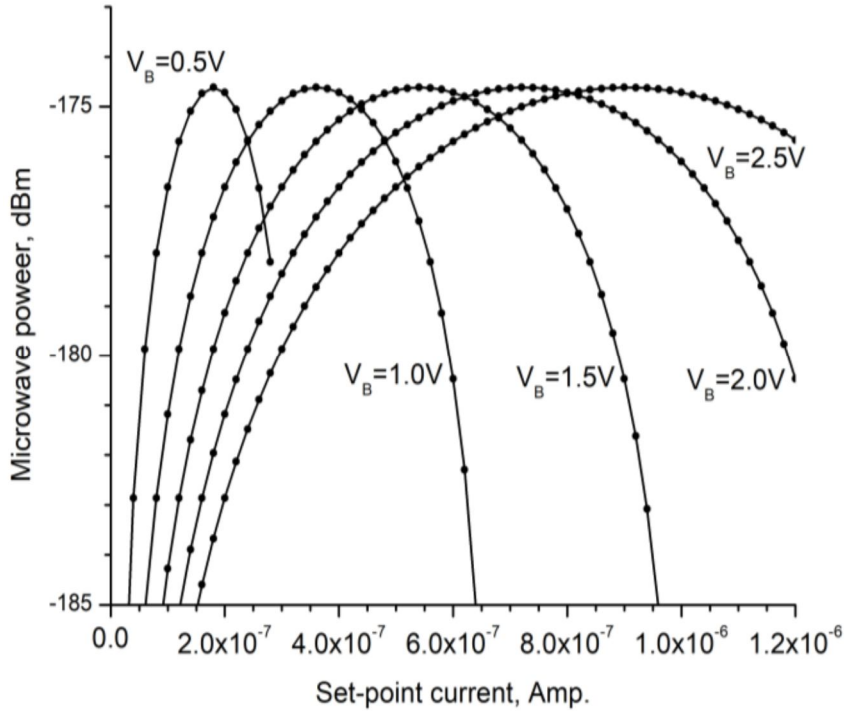


FIG. 6. Microwave power vs. DC tunneling current for specific values of the applied bias as calculated using Eq. (10) with $\rho = 0.1$ Ω-cm.

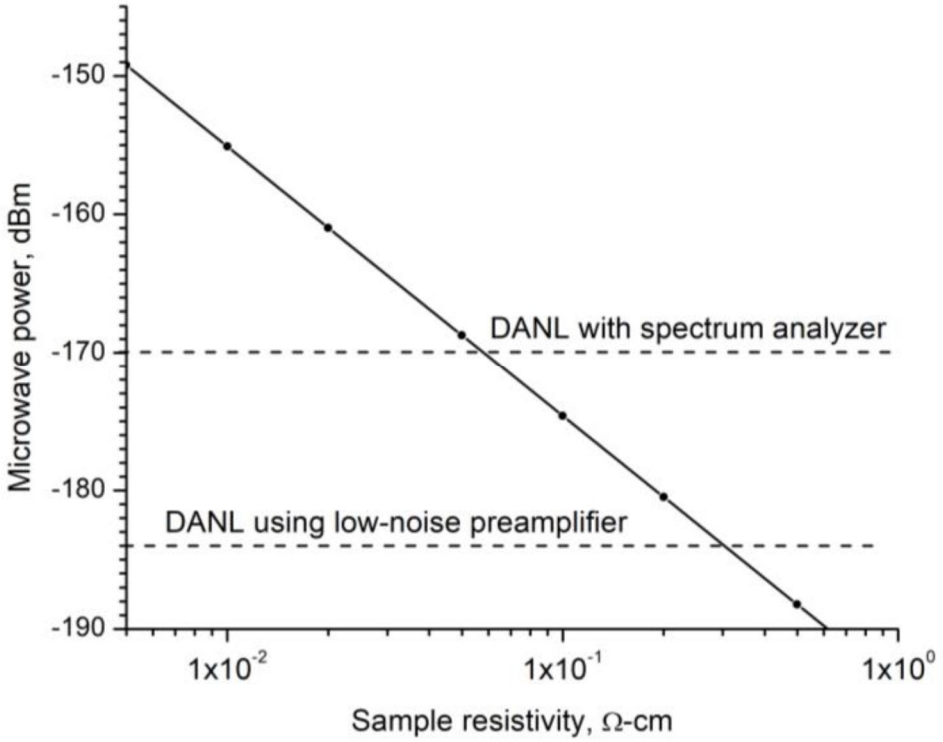


FIG. 7. Values for the microwave power, as a function of the sample resistivity, that are obtained by varying the applied DC bias and DC tunneling current to maximize the microwave power.

It may be seen in Fig. 7 that increasing the resistivity by a factor of 10 reduces the maximum possible microwave power by 19.5 dB, so that the maximum power varies approximately as the inverse square of the resistivity. For example, a 10% change in the resistivity of the sample would cause approximately a 20% change in the measured microwave power. Fig. 8 shows simulated values of the applied DC bias as a function of the DC current that give the maximum power at sample resistivities of 1.0, 0.5, 0.2, 0.1, 0.05, 0.02, 0.01, and 0.005 Ω-cm, from the top to the bottom curve. The power at each of these resistivities is

-194.1, 188.2, -180.5, -174.6, -168.7, -161.0, -155.1, and -149.2 dBm, again from the top to the bottom curve, respectively. These calculations were made for a tungsten tip having an apex radius of 0.3 nm. The reduction seen in the microwave power when increasing the resistivity is consistent with that shown in Fig. 7. A best-fit of all of the data in Fig. 8 gives the following empirical equation:

$$V_B = 2.60 \times 10^7 I_{SP} \rho^{0.975} \quad (11)$$

Figure 9 shows simulated values of the microwave power as a function of the tip-sample distance. The data correspond to three sets of simulations performed with DC currents of 10-8, 10-7, and 10-6 A, with the applied bias adjusted to maximize the power at each point. These calculations were made for a tungsten tip having an apex radius of 0.3 nm, with sample resistivities of 0.005, 0.010, 0.020, 0.050, 0.1, 0.2, 0.5, and 1 Ω-cm. Note that the three sets of data overlap in this figure.

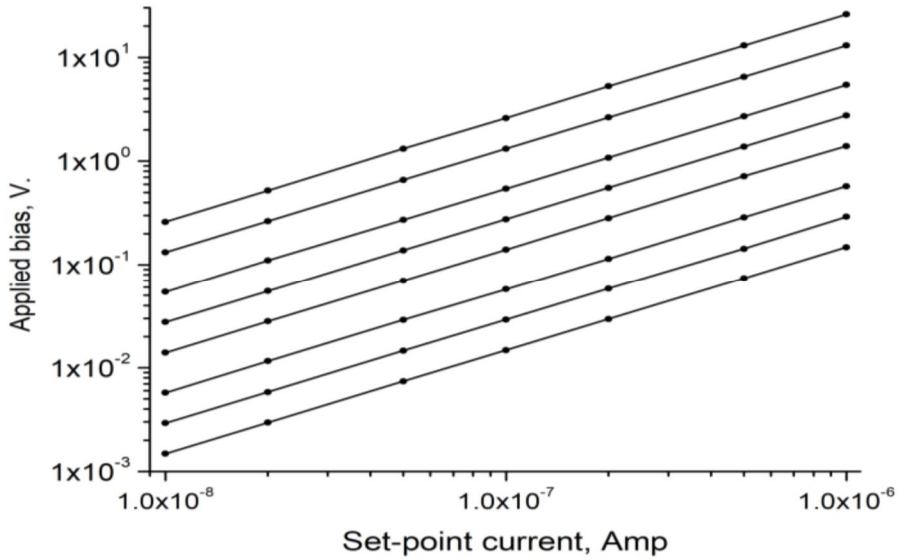


FIG. 8. Applied bias vs. current to obtain the maximum microwave power with sample resistivities of 1.0, 0.5, 0.2, 0.1, 0.05, 0.02, 0.01, and 0.005 Ω-cm. The power at each of these resistivities is -194.1, -188.2, -180.5, -174.6, -168.7, -161.0, -155.1, and -149.2 dBm from the top to the bottom of the 8 curves, respectively.

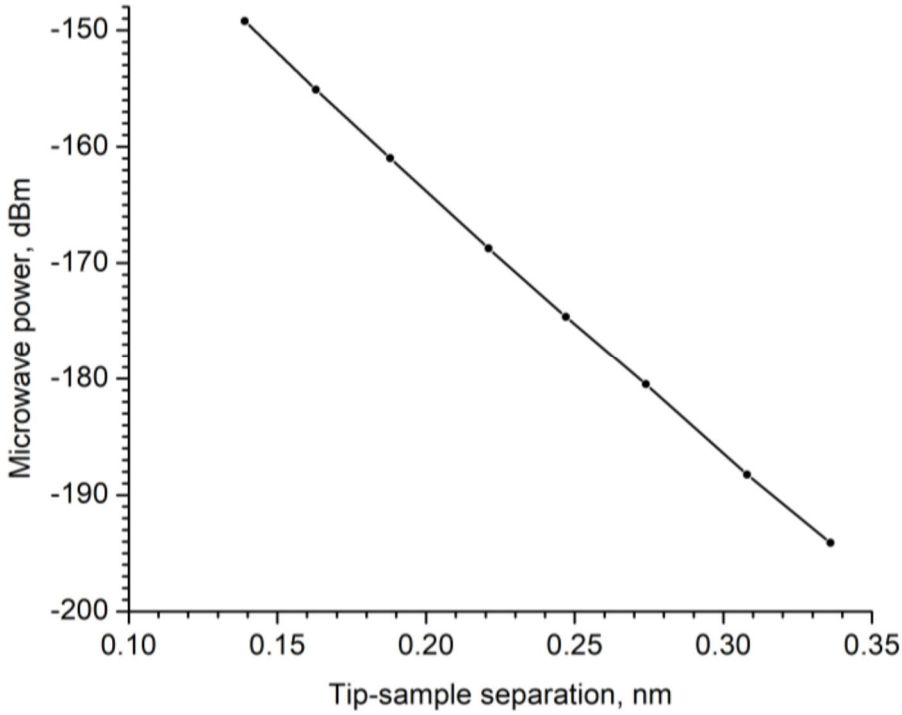


FIG. 9. Microwave power vs. tip-sample distance for three sets of simulations in which the applied bias and the current were adjusted to maximize the power at each point.

## 6. Possible Applications

One possible application of this technology is improved metrology for semiconductor devices. Roadmaps for the semiconductor industry request that the carrier concentration be measured with a resolution finer than 10 percent of the dimension at each lithography node. Scanning Spreading Resistance Microscopy (SSRM) is generally the method of choice for carrier profiling of semiconductor devices at and below the 20-nm lithography node in the semiconductor industry [11]. However, the diamond probes used to measure the spreading resistance in SSRM have an initial diameter of 10-15 nm that blunts to 50 nm or more during a single set of measurements [12], so this method fails to satisfy the roadmaps at the 12 and 20 nm nodes, which are now in production. We propose to develop new instrumentation for carrier profiling that is based on laser-assisted scanning tunneling microscopy, using a tunneling junction in place of the probes in SSRM, to provide sub-nm resolution while mitigating damage to the semiconductor. We would use a substitution method analogous to that already used to interpret the data in SSRM [12]. We would measure the power of the harmonics in the MFC by consecutive measurements with the test samples and standards under the same conditions of laser power, DC tunneling current, and many other parameters. We would use standards such as those already used with SSRM, which are silicon wafers with multiple sections having different known values for the carrier concentration [13]. Each sample and each standard would be cleaved and prepared with the same cleaning processes in order to compare each test sample with the standards under controlled conditions.

## 7. Conclusions

For each value of the DC applied bias, the DC tunneling current may be adjusted to maximize the microwave power. Also, for each value of the DC tunneling current, the DC applied bias may be adjusted to maximize the microwave power. In both cases, the maximum value for the microwave power and the value of the tip-sample distance at which it occurs are uniquely determined by the resistivity of the sample. The microwave power is generated by the nonlinear interaction of the incident laser radiation with the tunneling junction. The function of the DC tunneling current and the DC applied bias is to adjust the tip-sample distance so that the microwave power is maximized for a specific value of the sample resistivity. We are concerned about the apparent need for high DC tunneling currents when measuring the MFC with semiconductors. In our most recent measurements, scanning electron microscope (SEM) images show that the tip electrode is generally damaged at the end of each session of measurements. In our earlier measurements [4] we attribute the sudden onset of the harmonics as the DC bias was slowly increased to 9 V to the consequent reduction in the tip-sample distance, and attribute the relatively long period of time (43 minutes) in which the first 5 harmonics were measured to the gradual increase in this distance as the DC bias was slowly reduced to 5 V. The subsequent failure to detect the harmonics in that session was probably caused by a tip-crash. In tip-enhanced near-field Raman microscopy, a metal tip acts as an optical nanoantenna for near-field enhancement of the incident laser radiation at a spot of interest on the sample to obtain stronger signals and sub-nm resolution with the Raman effect [8]. By analogy, in laser-assisted scanning tunneling microscopy, the near-field enhancement of the optical radiation within the tunneling junction is strongly dependent on the tip-sample distance and the sharpness of the tip, so the resolution in imaging and the microwave power are strongly dependent on the placement of the tip and its sharpness. This shows the importance of optimizing the DC tunneling current and the applied DC bias voltage to avoid damaging the tip while obtaining the maximum microwave power and resolution.

## 8. Acknowledgments

This work is supported by the National Science Foundation under Grant 1648811.

## Appendix I. Approximation of the Spreading Resistance

The following three equations, corresponding to Eq. 25 in Ref. [6] by Simmons, give the tunneling current density J between two parallel metal plates, where a factor of 3/2 is deleted as a typographical error [14]. From symmetry, this may be used to determine the tunneling current density between two infinitesimal objects. Here, V is the potential difference, d is the distance, m and e are the mass and charge of the electron, h

is the Planck constant, and φM is the mean of the work functions for the two infinitesimal objects.

$$J = \alpha \frac{V_{TS}}{d} e^{-\beta d} \quad \text{(A1-1)}$$

Where $\alpha = \sqrt{2m\varphi_M e}\left(\frac{e}{h}\right)^2$ (A1-2)

And $\beta = \frac{4\pi}{h}\sqrt{2m\varphi_M e}$ (A1-3)

Earlier, our group developed a method to determine the radial distribution of the tunneling current at the surface of a metal sample in an STM [7] as an extension of the analysis by Simmons. We model the hemispherical apex of the tip electrode, having radius R, to be on the z-axis with z = d in cylindrical coordinates. The surface of the sample is at z = 0, so the tunneling current in the annulus with rmin < r < rmax is given by the following expression:

$$I_{DC} = 2\pi\alpha V_{TS} \int_{r_{min}}^{r_{max}} \frac{e^{-\beta s}}{s} r dr \quad \text{(A1-4)}$$

Where $s = \sqrt{r^2 + d^2} - R$ (A1-5)

Later, we also used Eq. (A1-4) to determine the total tunneling current and its distribution at the surface of a resistive sample. In this method, we approximate the current distribution by a radial hat (chapeau) function having width "a" that is called the "spot radius", defined to contain one-half of the total current in the distribution, and setting the height to contain the total current in the distribution. This is equivalent to approximating the current distribution for a metal disk having radius a at the surface of a flat slab with resistivity ρ when the radius of the disk is much less than the thickness of the slab. Thus, we approximate the spreading resistance by using the following expression, which is appropriate for a metal disc [5]:

$$R_s = \frac{\rho}{4a} \quad \text{(A1-6)}$$

Now we have used this procedure to generate a database consisting of a matrix with 12 values for the tip radius from 0.05 to 0.60 nm in steps of 0.05 nm, and 40 values of the tip-sample distance from 0.1 to 4.0 nm in 0.1 nm steps. In order to provide a simpler method to approximate the spreading resistance, we have used Eqs. (A1-7), (A1-8), and (A1-9), determining their four numerical parameters to obtain a best fit of the database, in which the errors have a mean magnitude of 6.4 percent and a maximum of 21.7 percent for the full set. Here, the spreading resistance RS (Ω) is given as a function of the resistivity of the sample ρ in Ω-cm, with the radius of the tip electrode R, and the tip-sample distance d (both in meters).

For example, with R = 4x10-10 m, F1(R) = -5.936x108 m-1 and F2(R,ρ) = 1.414x107 Ω. Then, Eqs. (A1-7)-(A1-9) may be used to show that, for ρ = 1 Ω-cm and d = 3x10-10 m, the spreading resistance RS = 11.8 MΩ.

$$F_1(R) = 4.773 \times 10^9 + 2.480 \times 10^8 Ln(R) \quad \text{(A1-7)}$$

$$F_2(R,\rho) = \frac{2462\rho}{R^{0.400}} \quad \text{(A1-8)}$$

$$R_s = F_2(R,\rho) \cdot e^{F_1(R)\cdot d} \quad \text{(A1-9)}$$

## Appendix II. Derivation of the Harmonics with a Semiconductor Sample

The following three equations, corresponding to Eq. 25 in reference [6] by Simmons, give the tunneling current density J between two parallel metal plates, where a factor of 3/2 is deleted as a typographical error [14]. From symmetry, this may be used to determine the tunneling current density between two infinitesimal objects. Here, V is the potential difference, d is the distance, m and e are the mass and charge of the electron, h is the Planck constant, and φM is the mean of the work functions for the two infinitesimal objects.

$$J = \alpha \frac{V_{TS}}{d} e^{-\beta d} \quad \text{(A2-1)}$$

Where $\alpha = \sqrt{2m\varphi_M e}\left(\frac{e}{h}\right)^2$ (A2-2)

And $\beta = \frac{4\pi}{h}\sqrt{2m\varphi_M e}$ (A2-3)

We extend the analysis by Simmons to approximate the DC tunneling current in a scanning tunneling microscope (STM), where the second and third terms within the brackets complete a power series to be consistent with measurements of the tunneling current vs. voltage in scanning tunneling spectroscopy. Here, A is the effective emitting area of the tip, and C > B2/4 because the DC tunneling current has the same sign as the bias voltage:

$$I_{DC} = \frac{\alpha A V_B}{d} e^{-\beta d}[1 + BV_B + CV_B{}^2] \quad \text{(A2-4)}$$

Equation (A2-4) is also a reasonable approximation for the DC tunneling current, even in the limit as the length of the leads to the tunneling junction is reduced to approach zero, where quasistatic approximations are

appropriate. Thus, we also use this equation at microwave and optical frequencies, following the approach that we have used previously to determine the linewidth for the harmonics of the MFC when using a metallic sample in an STM [2].

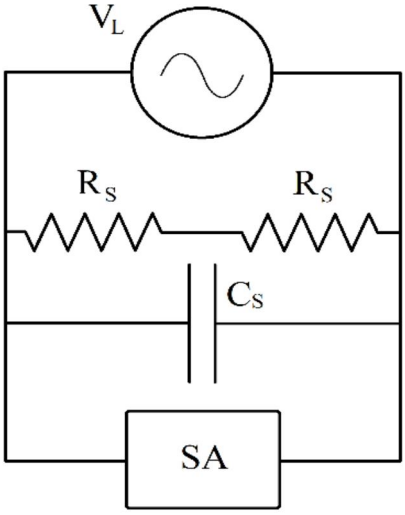


FIG. A2-1. Equivalent circuit for measuring the microwave frequency comb when the laser is focused on both the tunneling junction and the spreading resistance.

Figure A2-1 is the approximate high-frequency equivalent circuit for measuring the harmonics of the microwave frequency comb with a semiconductor sample. Then the high-frequency potential from the quasistatic electric field of the laser is imposed across the series combination of the tunneling resistance and the spreading resistance. Thus, the voltage drop across the spreading resistance reduces the voltage across the tunneling junction to attenuate the harmonics of the MFC. Then the high-frequency current through RT and RS in series is given by the following equation, where VT is the high-frequency potential across the tunneling resistance:

$$\mathrm{I(t)} = \frac{\alpha \mathrm{A}}{\mathrm{d}} \mathrm{e}^{-\beta \mathrm{d}} [\mathrm{V_T(t)} + BV_T(t)^2 + CV_T(t)^3] \quad \text{(A2-5)}$$

The tip electrode in an STM acts as an antenna in which a time-dependent feed-point voltage VL is received from the laser [6]. This potential is independent of the tip-sample distance because that distance is much less than the optical wavelength, so the optical electric field within the tunneling junction may be much greater than that in the incident field from the laser and varies inversely with the tip-sample distance. Now VL and VT are related by the following expression:

$$V_T + I(t)R_s = V_L(t) \quad \text{(A2-6)}$$

Combining Eqs. (A2-5) and (A2-6) gives the following expression in the voltage across the tunneling junction:

$$V_L(t) - V_T(t) = \frac{\alpha A R_S}{d} e^{-\beta d} [V_T(t) + BV_T(t)^2 + CV_T(t)^3] \quad \text{(A2-7)}$$

Assuming that a mode-locked laser is used with a long pulse sequence where each pulse is Gaussian with an effective width of τ, we express the time-dependent voltage across the tunneling junction by Eq. (A2-8), where the Cn are coefficients to be determined, ω0 is the optical frequency, and T is the time between consecutive laser pulses. The total voltage EL(t) is given by Eq. (A2-9).

$$V_T(t) = \sum_{-\infty}^{\infty} C_n e^{-\left(\frac{t-nT}{\tau}\right)^2} \cos[\omega_o(t-nT)] \quad \text{(A2-8)}$$

Substituting Eqs. (A2-6) and (A2-8) into Eq. (A2-7) gives the following equation where VL0 is the magnitude of VL:

$$\begin{aligned} &V_{L0} \sum_{-\infty}^{\infty} e^{-\left(\frac{t-nT}{\tau}\right)^2} \cos[\omega_o(t-nT)] - \\ &\sum_{-\infty}^{\infty} C_n e^{-\left(\frac{t-nT}{\tau}\right)^2} \cos[\omega_o(t-nT)] = \\ &\frac{\alpha A R_S}{d} e^{-\beta d} \left[ \sum_{-\infty}^{\infty} C_n e^{-\left(\frac{t-nT}{\tau}\right)^2} \cos[\omega_o(t-nT)] + \right. \\ &B \left[ \sum_{-\infty}^{\infty} C_n e^{-\left(\frac{t-nT}{\tau}\right)^2} \cos[\omega_o(t-nT)] \right]^2 + \\ &\left. C \left[ \sum_{-\infty}^{\infty} C_n e^{-\left(\frac{t-nT}{\tau}\right)^2} \cos[\omega_o(t-nT)] \right]^3 \right] \end{aligned} \quad \text{(A2-9)}$$

Since τ << T, the double and triple products of the summations in Eq. (A2-9) are each equivalent to single summations as follows:

$$\begin{aligned} &V_{L0} \sum_{-\infty}^{\infty} e^{-\left(\frac{t-nT}{\tau}\right)^2} \cos[\omega_o(t-nT)] - \\ &\sum_{-\infty}^{\infty} C_n e^{-\left(\frac{t-nT}{\tau}\right)^2} \cos[\omega_o(t-nT)] = \\ &\frac{\alpha A R_S}{d} e^{-\beta d} \left[ \sum_{-\infty}^{\infty} \mathrm{C_n e^{-\left(\frac{t-nT}{\tau}\right)^2} \cos[\omega_o(t-nT)]} + \right. \\ &\mathrm{B} \sum_{-\infty}^{\infty} \mathrm{C_n{}^2 e^{-2\left(\frac{t-nT}{\tau}\right)^2} \cos^2[\omega_o(t-nT)]} + \\ &\left. \mathrm{C} \sum_{-\infty}^{\infty} \mathrm{C_n{}^3 e^{-3\left(\frac{t-nT}{\tau}\right)^2} \cos^3[\omega_o(t-nT)]} \right] \end{aligned} \quad \text{(A2-10)}$$

Using trigonometric identities to simplify the square and cube of the cosine functions:

$$V_{L0}\sum_{-\infty}^{\infty} e^{-\left(\frac{t-nT}{\tau}\right)^2}\cos[\omega_o(t-nT)] - \sum_{-\infty}^{\infty} C_n e^{-\left(\frac{t-nT}{\tau}\right)^2}\cos[\omega_o(t-nT)] = \frac{\alpha AR_S}{d}e^{-\beta d}\left[\sum_{-\infty}^{\infty} C_n e^{-\left(\frac{t-nT}{\tau}\right)^2}\cos[\omega_o(t-nT)] + \frac{B}{2}\sum_{-\infty}^{\infty} {C_n}^2 e^{-2\left(\frac{t-nT}{\tau}\right)^2}[1+\cos[2\omega_o(t-nT)]] + \frac{C}{4}\sum_{-\infty}^{\infty} {C_n}^3 e^{-3\left(\frac{t-nT}{\tau}\right)^2}[3\cos[\omega_o(t-nT)]]+\cos[3\omega_o(t-nT)]\right] \quad \text{(A2-11)}$$

Deleting all terms at frequencies other than the optical frequency gives the following expression:

$$V_{L0}\sum_{-\infty}^{\infty} e^{-\left(\frac{t-nT}{\tau}\right)^2}\cos[\omega_o(t-nT)] - \sum_{-\infty}^{\infty} C_n e^{-\left(\frac{t-nT}{\tau}\right)^2}\cos[\omega_o(t-nT)] = \frac{\alpha AR_S}{d}e^{-\beta d}\left[\sum_{-\infty}^{\infty} C_n e^{-\left(\frac{t-nT}{\tau}\right)^2}\cos[\omega_o(t-nT)] + \frac{3C}{4}\sum_{-\infty}^{\infty} {C_n}^3 e^{-3\left(\frac{t-nT}{\tau}\right)^2}\cos[\omega_o(t-nT)]\right] \quad \text{(A2-12)}$$

Rearranging the terms in Eq. (A2-12) gives the following expression:

$$\sum_{-\infty}^{\infty}\left[V_{L0}e^{-\left(\frac{t-nT}{\tau}\right)^2} - C_n e^{-\left(\frac{t-nT}{\tau}\right)^2} - \frac{\alpha AR_S}{d}e^{-\beta d}C_n e^{-\left(\frac{t-nT}{\tau}\right)^2} - \frac{3C\alpha AR_S}{4d}e^{-\beta d}{C_n}^3 e^{-3\left(\frac{t-nT}{\tau}\right)^2}\right]\cos[\omega_o(t-nT)] = 0 \quad \text{(A2-13)}$$

But Eq. (A2-13) must be satisfied at each value of n in the summation, with the additional approximation that the coefficient C may be deleted. Thus, we have Eq. (A2-14) for the coefficients, which is used with Eq. (A2-8) to obtain Eq. (A2-15) for the potential across the tunneling junction:

$$C_n = \frac{V_{L0}}{\left(1+\frac{\alpha AR_S}{d}e^{-\beta d}\right)} \quad \text{(A2-14)}$$

$$V_T(t) = \frac{V_{L0}}{\left(1+\frac{\alpha AR_S}{d}e^{-\beta d}\right)}\sum_{-\infty}^{\infty} e^{-\left(\frac{t-nT}{\tau}\right)^2}\cos[\omega_o(t-nT)] \quad \text{(A2-15)}$$

Next, Eqs. (A2-5) and (A2-15) are combined to obtain Eq. (A2-16) for the current:

$$I(t) = \frac{\alpha A}{d}e^{-\beta d}\left[\frac{V_{L0}}{\left(1+\frac{\alpha AR_S}{d}e^{-\beta d}\right)}\sum_{-\infty}^{\infty} e^{-\left(\frac{t-nT}{\tau}\right)^2}\cos[\omega_o(t-nT)] + B\frac{{V_{L0}}^2}{\left(1+\frac{\alpha AR_S}{d}e^{-\beta d}\right)^2}\left[\sum_{-\infty}^{\infty} e^{-\left(\frac{t-nT}{\tau}\right)^2}\cos[\omega_o(t-nT)]\right]^2 + C\frac{{V_{L0}}^3}{\left(1+\frac{\alpha AR_S}{d}e^{-\beta d}\right)^3}\left[\sum_{-\infty}^{\infty} e^{-\left(\frac{t-nT}{\tau}\right)^2}\cos[\omega_o(t-nT)]\right]^3\right] \quad \text{(A2-16)}$$

Since $\tau << T$, the double and triple products of the summations in Eq. (A2-16) are each equivalent to single summations as follows:

$$I(t) = \frac{\alpha A}{d}e^{-\beta d}\left[\frac{V_{L0}}{\left(1+\frac{\alpha AR_S}{d}e^{-\beta d}\right)}\sum_{-\infty}^{\infty} e^{-\left(\frac{t-nT}{\tau}\right)^2}\cos[\omega_o(t-nT)] + B\frac{{V_{L0}}^2}{\left(1+\frac{\alpha AR_S}{d}e^{-\beta d}\right)^2}\left[\sum_{-\infty}^{\infty} e^{-2\left(\frac{t-nT}{\tau}\right)^2}\cos^2[\omega_o(t-nT)]\right] + C\frac{{V_{L0}}^3}{\left(1+\frac{\alpha AR_S}{d}e^{-\beta d}\right)^3}\left[\sum_{-\infty}^{\infty} e^{-3\left(\frac{t-nT}{\tau}\right)^2}\cos^3[\omega_o(t-nT)]\right]\right] \quad \text{(A2-17)}$$

Using trigonometric identities to simplify the square and cube of the cosine functions:

$$I(t) = \frac{\alpha A}{d}e^{-\beta d}\left[\frac{V_{L0}}{\left(1+\frac{\alpha AR_S}{d}e^{-\beta d}\right)}\sum_{-\infty}^{\infty} e^{-\left(\frac{t-nT}{\tau}\right)^2}\cos[\omega_o(t-nT)] + \frac{B}{2}\frac{{V_{L0}}^2}{\left(1+\frac{\alpha AR_S}{d}e^{-\beta d}\right)^2}\left[\sum_{-\infty}^{\infty} e^{-2\left(\frac{t-nT}{\tau}\right)^2}[1+\cos[2\omega_o(t-nT)]]\right] + \frac{C}{4}\frac{{V_{L0}}^3}{\left(1+\frac{\alpha AR_S}{d}e^{-\beta d}\right)^3}\left[\sum_{-\infty}^{\infty} e^{-3\left(\frac{t-nT}{\tau}\right)^2}[3\cos[\omega_o(t-nT)]+\cos[3\omega_o(t-nT)]]\right]\right] \quad \text{(A2-18)}$$

The objective is to determine the harmonics of the MFC in RT and RS so that all terms in Eq. (A2-18) that are at or above the optical frequency are deleted to give the following expression:

$$I(t) = \frac{1}{\left(1+\frac{\alpha AR_S}{d}e^{-\beta d}\right)^2}\frac{\alpha AB{V_{L0}}^2}{d}e^{-\beta d}\sum_{-\infty}^{\infty} e^{-2\left(\frac{t-nT}{\tau}\right)^2} \quad \text{(A2-19)}$$

Thus, we obtain Eq. (A2-20) for the power at the nth harmonic, which may be written in the form of Eq. A2-21) to show the effect of the ratio of the spreading resistance to the tunneling resistance.

$$P_n) = \frac{1}{\left(1+\frac{\alpha AR_S}{d}e^{-\beta d}\right)^4}\frac{\pi\alpha^2A^2B^2{V_{L0}}^4e^{-\beta d}}{4d^2\left[1+\left(\frac{2n\pi}{T}R_{SA}C_S\right)^2\right]}\left(\frac{\tau}{T}\right)^2 \quad \text{(A2-20)}$$

$$P_n) = \frac{1}{\left(1+\frac{R_S}{R_T}\right)^4} \frac{\pi\alpha^2 A^2 B^2 {V_{L0}}^4 e^{-\beta d}}{4d^2\left[1+\left(\frac{2n\pi}{T}R_{SA}C_S\right)^2\right]} \left(\frac{\tau}{T}\right)^2 \quad \text{(A2-21)}$$

In the main body of this documentation, we alluded to the possibility of using a substitution method to determine the spreading resistance, and thus the carrier concentration of a sample, instead of making an absolute determination of the carrier density. That is, we would determine the carrier concentration by comparing measurements of the power at one or more of the harmonics in the MFC with test samples to measurements made with a group of standards under the same conditions of laser power, DC tunneling current, and the other parameters.

In order to examine the possibility of using a substitution method, we write Eq. (A2-21) in the form of Eq. (A2-22), where G will have the same value for the test samples and the standard samples having known resistivities. Thus, if the test samples and the standards are measured at the same harmonic, the microwave power will be proportional to the prefactor γ, defined in Eq. (A2-23). Procedures for determining the resistivity from these measurements by using the prefactor are described in the body of this documentation.

$$P_n = \gamma \mathrm{F(n)G} \quad \text{(A2-22)}$$

$$\gamma = \frac{e^{-2\beta d}}{d^2\left(1+\frac{R_S}{R_T}\right)^4} \quad \text{(A2-23)}$$

$$\mathrm{F(n)} = \frac{1}{1+\left(\frac{2n\pi}{T}R_{SA}C_S\right)^2} \quad \text{(A2-24)}$$

$$G = \frac{\pi}{4}\alpha^2 A^2 B^2 {E_{L0}}^4 \left(\frac{\tau}{T}\right)^2 \quad \text{(A2-25)}$$

## References:


[1] Hagmann, M.J., Taylor, A.J., and Yarotski, D.A., Appl. Phys. Lett., 101 (2012) 241102.

[2] Hagmann, M.J., Stenger, F.S., and Yarotski, D.A., J. Appl. Phys., 114 (2013) 223107.

[3] Hagmann, M.J., Coombs, D.G., and Yarotski, D.A., J. Vac. Sci. Technol. B, 35 (2017) 03D109.

[4] Rhoades, C., Rasmussen, J., Bowles, P.H., Hagmann, M.J., and Yarotski, D.A., Proc. 2016 IEEE Workshop on Microelectronics and Electron Devices, 4 pp.

[5] Gelmont, B. and Shur, M., Solid-State Electron., 36 (1993) 143.

[6] Simmons, J.G., J. Appl. Phys., 34 (1963) 1793.

[7] Hagmann, M.J. and Henage, T.E., Electron. Lett., 52 (2016) 395.

[8] Shi, X., Coca-Lopez, N., Janik, J., and Hartschuh, A., Chem. Rev., 117 (2017) 4945.

[9] Zhu, C., Andrei, P., and Hagmann, M.J., Proc. 2017 IEEE Workshop on Microelectronics and Electron Devices, 4 pp.

[10] Hagmann, M.J., Pandey, S., Nahata, A., Taylor, A.J., and Yarotski, D.A., Appl. Phys. Lett., 101 (2012) 231102.

[11] Vandervorst, W., Schultze, A., Kambham, A.K., Mody, J., Gilbert, M., and Eyben, P., Phys. Status Solidi C, 11 (2014) 121.

[12] Hantschel, T., Tsigkourakos, M., Kluge, J., Werner, T., Zha, L., Paredis, K., Eyben, P., Nuytten, T., Xu, Z., and Vandervorst, W., Microelectron. Eng., 141 (2015) 1.

[13] IMEC, Scanning Spreading Resistance Microscopy Standards SSRM-SMPL-N and SSRM-SMPL-P, available at www.brukerafmprobes.com.

[14] Matthews, N., Hagmann, M.J., and Mayer, A., J. App. Phys., 123 (2018) 13601.